BULLETIN OF THE POLISH ACADEMY OF SCIENCES
TECHNICAL SCIENCES, Vol. 58, No. 4, 2010
DOI: 10.2478/v10175-010-0073-8

Analysis of the stress state in the harmonic drive generator-flexspline system in relation to selected structural parameters and manufacturing deviations

W. OSTAPSKI*

Institute of Machine Design Fundamentals, Warsaw University of Technology, 84 Narbutta St., 02-524 Warszawa, Poland

Abstract. In the paper, the problem of failure of the elastic bearing supporting the generator in a harmonic drive is presented. To analyse the cause of the failure, material investigations as well as simulations of the stress state in the bearing versus manufacturing deviations and fits between the bearing and the generator cam have been carried out. Studies on the stress state in the flexpline have also been conducted in dependence of such technological deviations and generator bearing-flexspline fits for the classical, short, and ultra-short version of the harmonic drive with different heights of the bottom. The simulations have been realised on a mathematical model based on analytical relationships and a 3D model with the aid of FEM.

Key words: gear of harmonic drive, flexible rolling bearings, mathematical modelling, stress analysis, manufacturing deviations.

1. Analysis of the cam generator-flexible bearing association

Flexible rolling bearings designer for generators of harmonic drives are specialized bearings. High operational requirements, in particular reliability, stability in maintaining magnitude of radial clearance in operational conditions as well as silent-running feature call for great experience and high technology level of the manufacturer. Proper operation of the bearing of a harmonic drive needs securing an appropriate radial gap after assembling the bearing. A reliability test carried out on a HP80-83 harmonic drive with the generator bearing shown in Fig. 2 associated with the cam (Fig. 1) according to the source version (Table 1) was finished due to crack of the external ring of the bearing (Figs. 3–5). Material examinations did not reveal any deviations from chemical composition and the bearing manufacturing process (Sec. 2). The performed analysis of fit in particular cams with the LG8060 bearing delivered in the source version enabled the assessment of correctness of the associations with respect to the criterion of minimum radial clearance of the generator bearing. FEM simulations of a 3D generator model with a flexible bearing allowed one to determine the effect of the cam-bearing ring association quality on the stress state in the bearing. The problem was considered as multi-sided elastic contact. The bearing hole for the cam was $d = 60^{0}_{-0.015}$, theoretical inner radial clearance 0.03–0.05 mm. The tolerance of elastic radii in the figures was $R^{0.01}_{0.001}$. To obtain proper values of the radial gap in the cam fit with respect of stresses, some corrections were introduced to the harmonic drive HP80-83.

Calculations of subsequent associations and true limit clearance gave:

Table 1

Bearing $d = 60^{0}_{-0.015}$		
No. R	Ro – source version	Rn – corrected verion
1	$Ro = 29.9920 + 0.4880$	$Rn = 29.9790 + 0.4880$

The radius of the cam before correction for: $i = 83$, $m = 0.5$ mm, *Wo/m* $= 0.976$

$$R = 29.992 + 0.488\cos 2\varphi, \quad R^{0.01}_{0.001} \tag{1}$$

The inner diameter of the bearing: $d = 60^{0}_{-0.015}$ and the proposed change: $d = 60^{+0.015}_{0}$.

Table 2

Circumference for d		
Lo	$L_{-0.015}$	$L^{+0.015}$
188.49556	188.4484	188.5427

Table 3

Cam circumference with the radius before correction	
$L_{R+0.001}$	$L_{R+0.01}$
188.5019	188.5584

The cam radius after correction:

$$R = 29.979 + 0.488\cos 2\varphi, \quad R^{0.01}_{0.001}. \tag{2}$$

Table 4

Cam circumference after correction	
$L_{Rk+0.001}$	$L_{Rk+0.01}$
188.4705	188.5270

The description of the base bearing hole $d = 60^{0}_{-0.015}$ with the uncorrected cam radius $R^{0.01}_{0.001}$ are as follows (Tables 2–4):

*e-mail: wos@simr.pw.edu.pl

$$Lo - L_{R+0.001} = 188.49556{-}188.5019 = -0.00634 \text{ mm}$$

$$Lo - L_{R+0.01} = 188.49556{-}188.5584 = -0.06284 \text{ mm}$$

$$L_{-0.015} - L_{R+0.001} = 188.4484{-}188.5019 = -0.0535 \text{ mm}$$

$$L_{-0.015} - L_{R+0.01} = 188.4484{-}188.5584 = -0.11 \text{ mm} \quad (3)$$

In each of the above case there is interference and only the first value can be accepted as the other ones lead to elimination of the radial clearance, the 0.11 mm interference in particular.

The cam according to the producer data: $i = 83$, $m = 0.5$ mm, *Wo/m* $= 0.976$, *Wo* $= 0.488$, $R = 29.992 + 0.488\cos 2\varphi$.

The association of the base bearing hole $d = 60^{0}_{-0.015}$ with the corrected cam radius $R^{0.01}_{0.001}$ are as follows:

$$Lo - L_{Rk+0.001} = 188.49556 - 188.4705 = 0.0250$$

$$Lo - L_{Rk+0.01} = 188.49556 - 188.5270 = -0.0314$$

$$L_{-0.015} - L_{Rk+0.001} = 188.4484 - 188.4705 = -0.022$$

$$L_{-0.015} - L_{Rk+0.01} = 188.4484 - 188.5270 = -0.0786 \quad (4)$$

In the above case it is enough to select the bearings into two size groups to maintain the recommended fit for the internal bearing ring on the cam – the gap $0 \div 0.025$ on the diameter (the optimal association – 0.01–0.02).

The cam according to the producer data: $i = 83$, $m = 0.5$ mm, *Wo/m* $= 0.976$, *Wo* $= 0.488$, $R = 29.979 + 0.488\cos 2\varphi$.

Alternatively, it is possible to apply the H-fit for the bearing hole, i.e. $d = 60^{+0.015}_{0}$. Then relations appearing in the association of the base bearing hole $d = 60^{+0.015}_{0}$ with the cam with corrected radius $R^{0.01}_{0.001}$ are:

$$Lo - L_{Rk+0.001} = 0.0250 \text{ mm}$$

$$Lo - L_{Rk+0.01} = -0.0314 \text{ mm}$$

$$L^{+0.015} - L_{Rk+0.001} = 188.5427{-}188.4705 = 0.0720 \text{ mm}$$

$$L^{+0.015} - L_{Rk+0.01} = 188.5427{-}188.5270 = 0.0157 \text{ mm} \quad (5)$$

A selection through change of the second and third association yields the recommended values of the clearance.

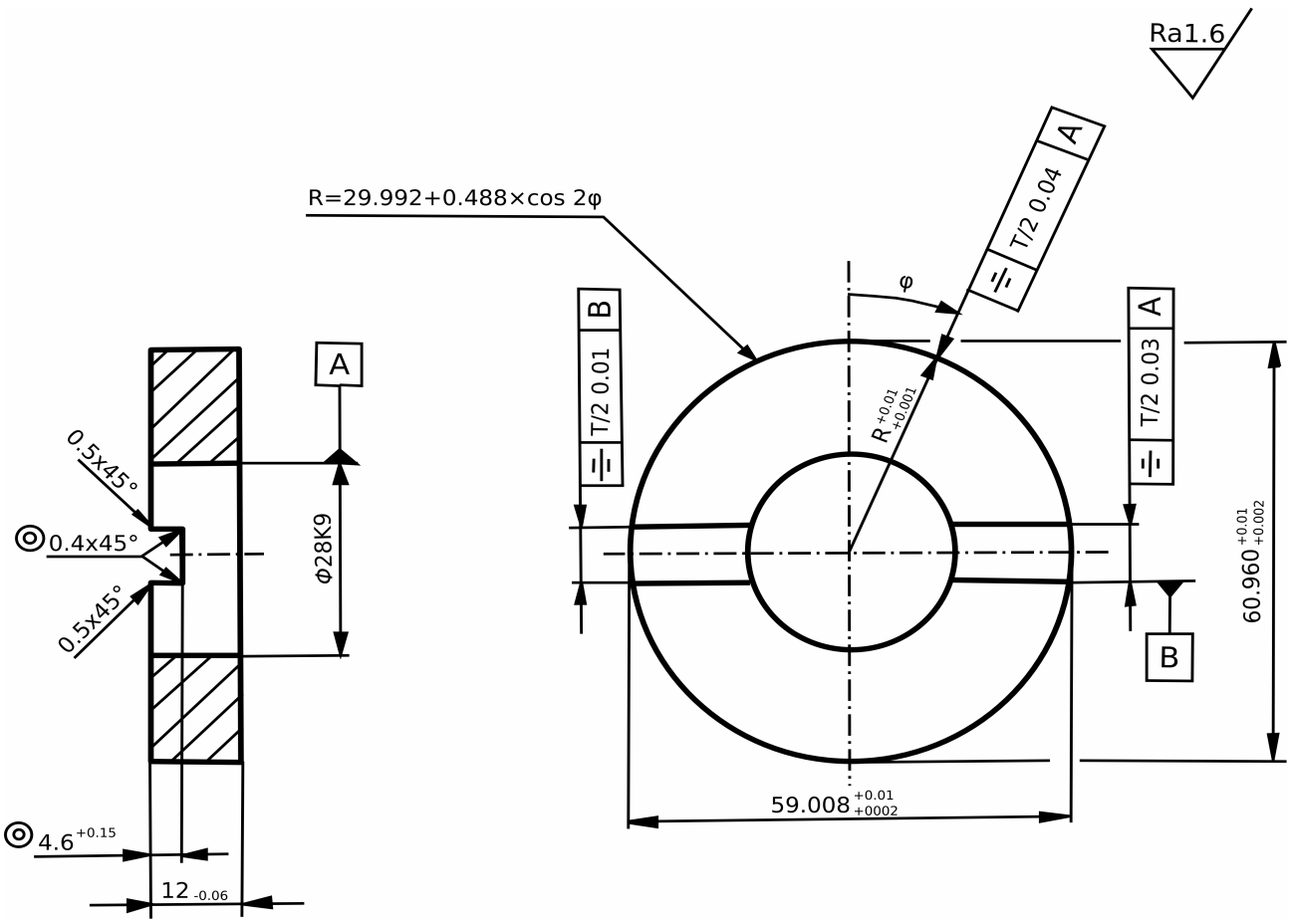

Fig. 1. Generator cam

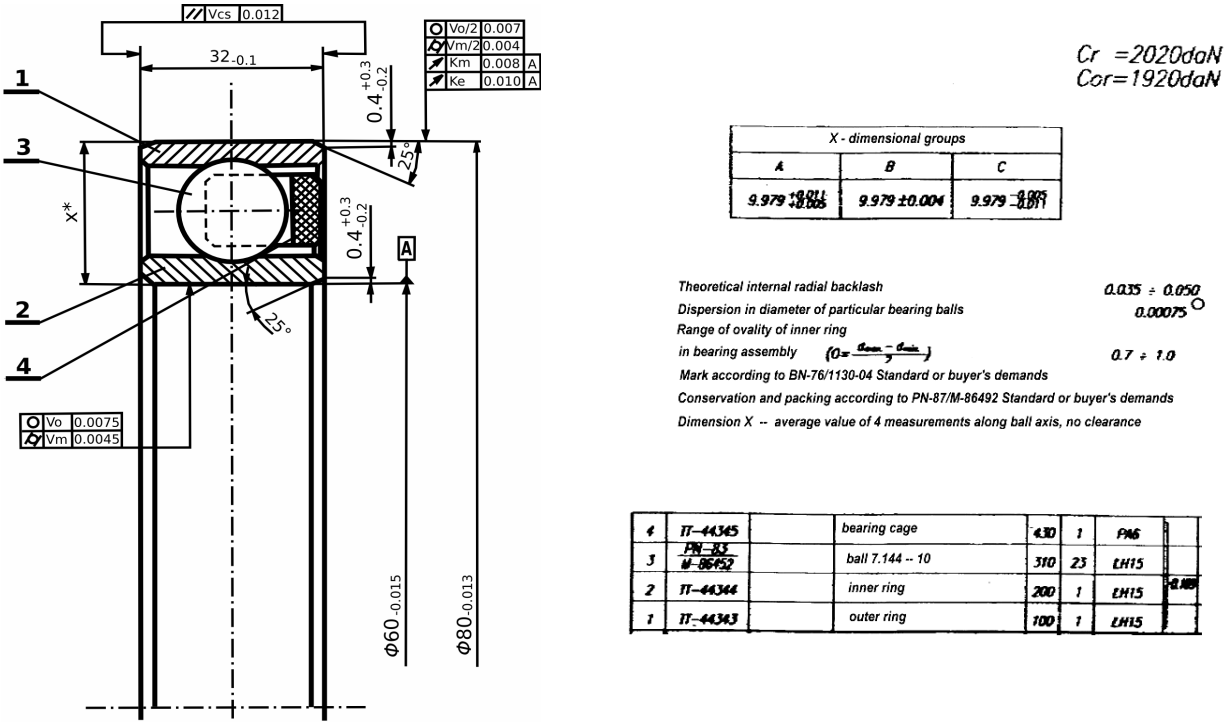

Fig. 2. Flexible bearing of the cam

2. Test-stand and material examinations of the harmonic drive bearing

The experimental loading of the HP80-83 harmonic drive was Mo =120–200 Nm at the angular speed of the generator shaft ng =1200–1500 rpm. The loading test $T = 72$ hrs equivalent to 1.16×10^7 cycles of average torque *Mrms* = 160 Nm was terminated after cracking of the external ring of the generator bearing (Figs. 3–5). Dimensional analysis of the considered structural node exhibited an interference of about 0.025–0.030 mm in the fit between the cam and the bearing. This practically eliminated or, at least, strongly limited the necessary radial clearance of the bearing in the extreme association, which led to excessive stress in the external ring and a high torque loading in the axial generator bearing. This way increased the normal stress in the external ring variable bilaterally due to bearing bending from the cam. Fitting the external ring with interference on the cam resulted in additional normal stresses brought about by tension in the internal ring as well as by elimination of the radial clearance. The bearing operates in hard loading conditions. Similarly as the classical rolling bearing, it is exposed to fatigue with respect to contact stresses and additionally with respect to bending of the internal ring (constant *pw*) and the external one (variable *pz*). Elimination of the clearance introduced additional stresses to both rings, but the external one working with accordance to the volume fatigue strength had lower durability than the internal ring subjected to constant volume stresses.

A program of material examinations (Table 5) for the external ring of the generator flexible bearing:

- Test of hardness – the required 58–61 HRC, measured – 60 HRC.
- Search for grinding burns – after etching and visual inspection no traces of grinding burns were detected.
- Microstructure examination – the specimen was cut out from the ring, polished, etched in nital and assessed according to WTc-1 conditions of technical inspection of the material manufacturer.

Table 5

Examined parametr of microstructure	Requirements	Results
martensite	2–6	4
dispersion of carbides	3.3a–5.5a	3.3a
carbide network	max 3	1
segregation of carbides	max 6.2	6.0
carbide banding	max 7.3	7.1

No non-metallic contaminations were found in the not etched metallographic section.

- Examination of the chemical composition (Table 6).

Table 6

Alloy element	Requirements	Results
C	0.90–1.05	0.92
Mn	0.25–0.45	0.28
Si	0.15–0.35	0.25
P	max 0.025	0.003
S	max 0.015	0.003
Cr	1.35–1.65	1.55
Ni	max 0.30	0.11
Mo	max 0.10	0.02
Cu	max 0.25	0.15
Al	0.010–0.050	0.033
Ti(ppm)	max 30	30ppm

Summarising the material investigations, one can conclude that:

- No deviations from technical conditions and requirements were found.
- Identations and deformations on the outer surface of the external ring occurred after crack of the ring.
- Local deformation of the external ring may result from contact with the damaged toothed ring of the harmonic drive flexspline.
- Technological deviations and the clearance in the association cam-bearing-flexspline should be verified.

a)

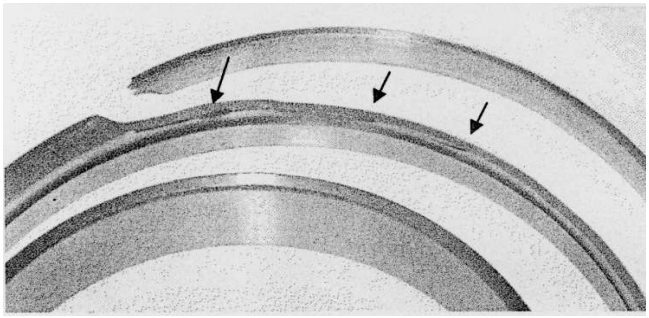

b)

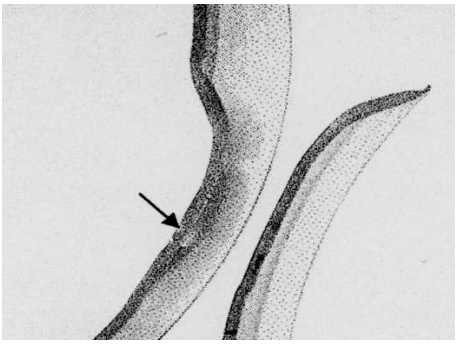

Fig. 3. a) Bearing ring – traces of identation due to balls on the running track *pz*, b) local deformation on the outer surface of the external ring

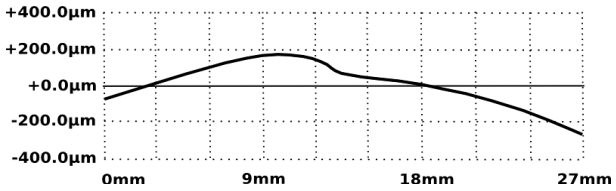

Fig. 4. Graph of the local deformation of the outer surface *pz*

During repeated overloadings of the harmonic drive within the range of k=2Mnom and in the case of fitting the cam on the bearing with the allowable clearance, there may appear relative displacement between the cam and the internal bearing ring. This leads to abrasive wear and micro-spalling intensified by the lubricant that penetrates micro-cracks and thus accelerates pitting of the bearing running tracks. Such an association of the internal ring of the generator and the cam acts as a micro-pump sucking the lubricant fluid in the area of minor axes of the cam (outside the meshing zone) and as a compressing micro-press in the area of the major axis, where the bearing loading from the radial component of meshing forces reaches its maximum. An effect of such an action is shown in Fig. 6. This is a cam of a $M\mathrm{nom} = 800$ Nm harmonic drive examined for durability on the test stand at the Institute of Machine Design Fundamentals at Warsaw University of Technology. The applied loading and testing time was equivalent to 15 thousand hours of operation in nominal conditions. The maximum instantaneous loading was $M\max = 1600$ Nm, time of duration $T = 3$ s, frequency – 5 overloadings per hour.

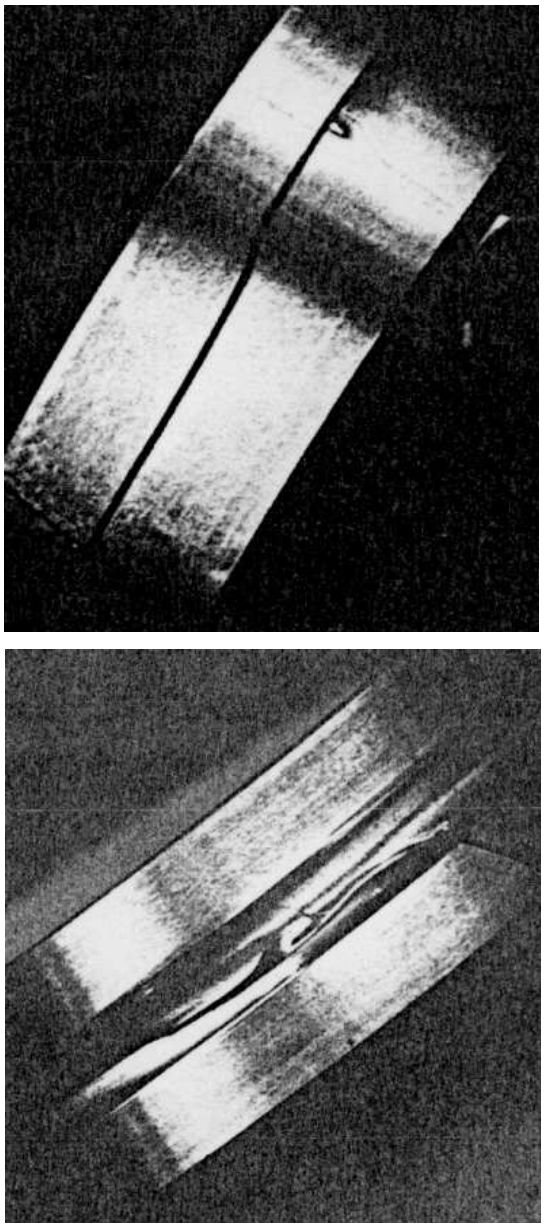

Fig. 5. View of a damaged bearing

The flexible bearing (Fig. 6) of the generator works in a complex state of loading. In order to determine its durability for the assumed operational conditions or find parameters for the complex durability, it is necessary to establish the

magnitude and course of the bearing loading in function of the torque applied to the harmonic drive. At the same time, the type of flexspline design, kind and teeth geometry, torsional stiffness of the drive and the generator-flexspline node as well as the accuracy class should be kept in mind. [1]. The bearing is expanded from the inside, it is compressed by the radial components of meshing forces acting in two zones (bi-harmonic drive). Both components of the radial meshing forces are balanced by the reaction of the bearing. Owing to torsional flexibility of the drive and true manufacturing deviations, both zones of radial meshing forces lose their symmetry with respect to the cam axis and the cam reaction forces during growth of the loading carried on by the drive. In dynamical conditions of operation, reversals and overloadings, this phenomenon intensifies itself. A local loss of contact between the flexspline and the external bearing ring as well as an increase in flexspline stresses take place in two areas rotated from the major cam axis in the in opposite direction with respect to velocity of the generator [2]. This undesirably affects the durability of the flexible bearing as it leads to generation of transverse vibration (radial movements of the cam in the Oldhamm coupling) and induced by it torsional vibration of the generator. This, in turn, disturbs motion of the rolling elements, which produces transverse vibration, braking, slip, increase of friction, non-uniformity of loading of the rolling elements and, finally, growth of noise. As a result, the durability of the bearing and the harmonic drive itself lowers.

Fig. 6. Flexible bearing fitted with clearance on the cam

3. 3D FEM model of the cam generator

In order to carry radial interactions between the bearing balls and running tracks, in the complete model node-to-node contacts were applied. This represents a purely point-like contact that was incorporated to diminish the computational size of the model. Such kind of contact enables taking into consideration the radial clearance or interference (in the model the gap was 0.03 mm), see Fig. 7.

FEM simulation results ($R_{run} = 0.525 * \phi_{ball}$, $R = 29.992 + 0.488\cos(2\phi)$ minimum interference after correction of the fit).

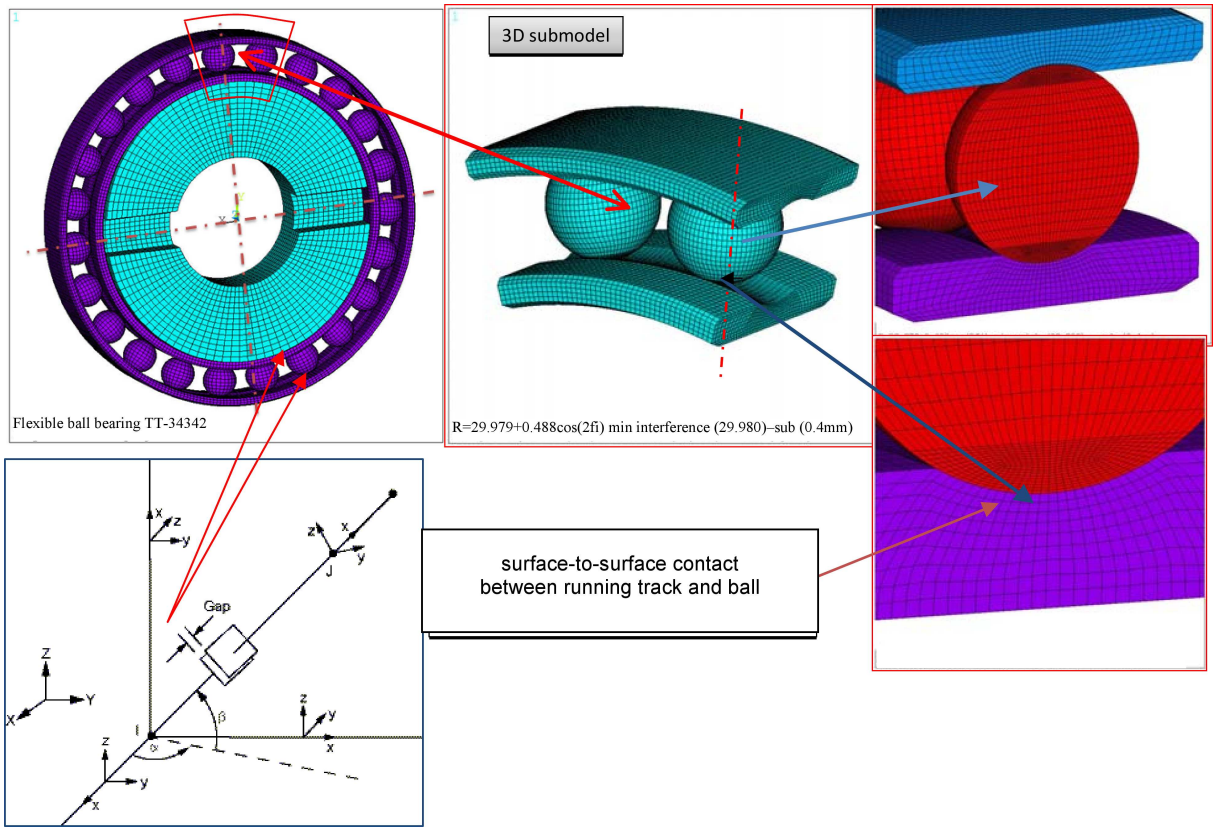

Fig. 7. FEM model of the bearing assembly

a) b)

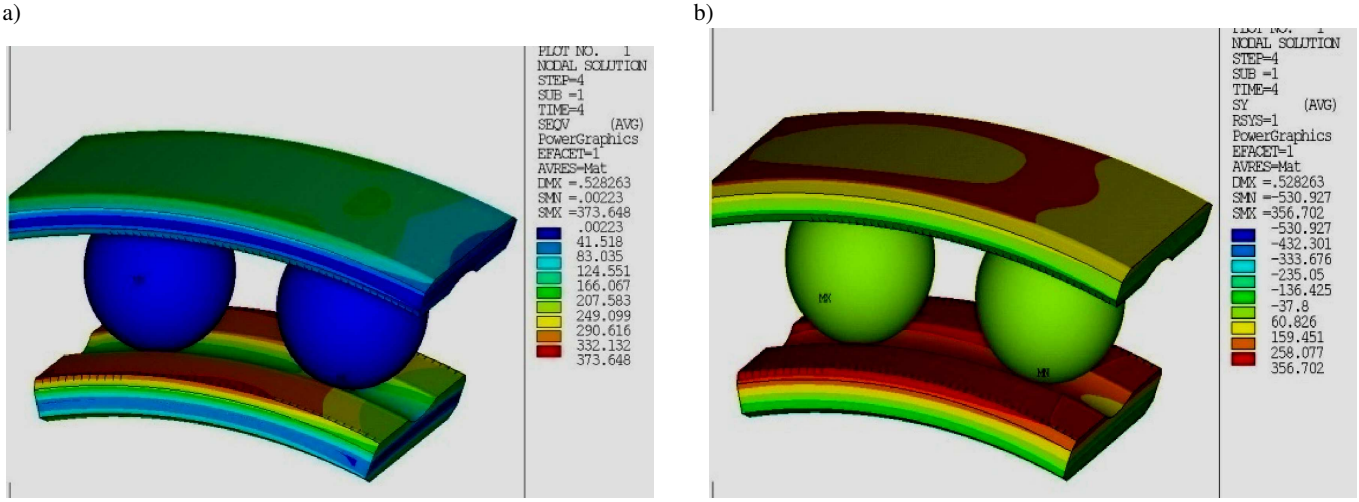

Fig. 8. Stresses: a) Huber-Mises, b) circumferential

a) b)

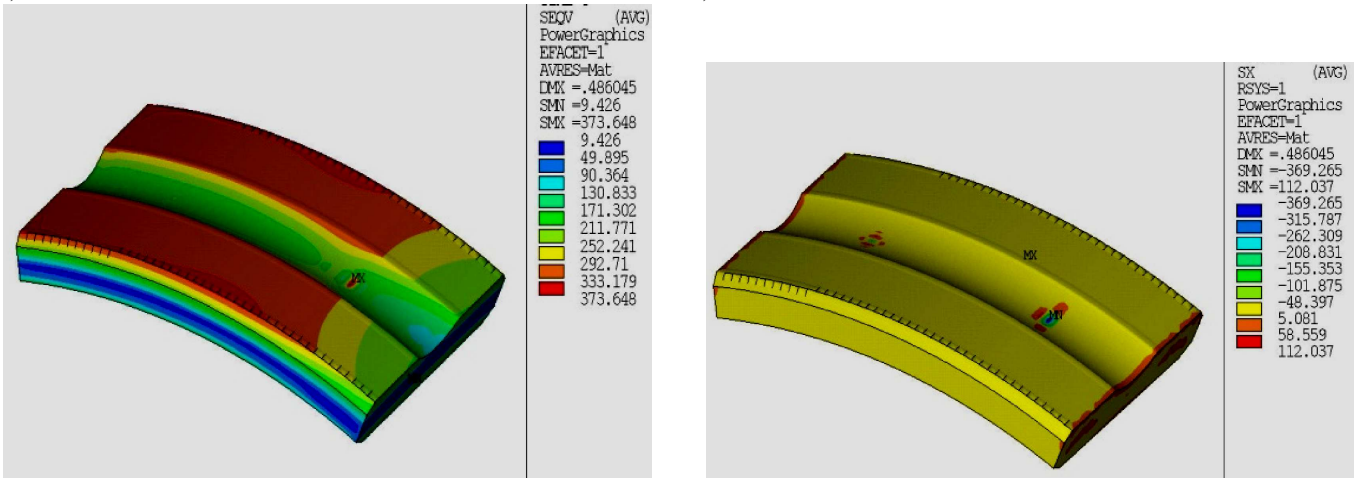

Fig. 9. Stresses on the inside running track: a) Huber-Mises, b) radial

a) b)

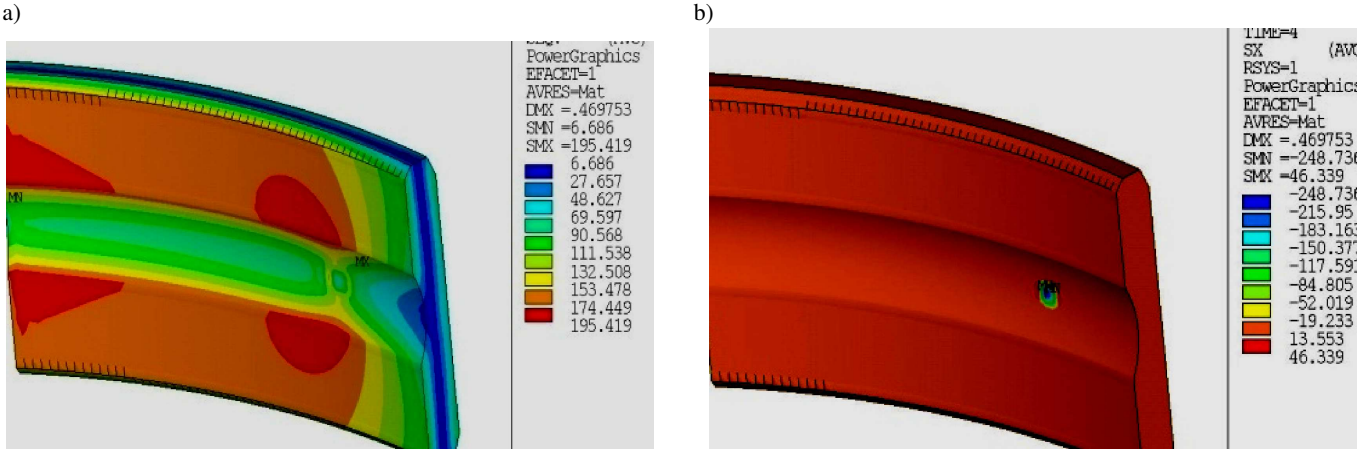

Fig. 10. Stresses on the outside running track: a) Huber-Mises, b) radial

a) b)

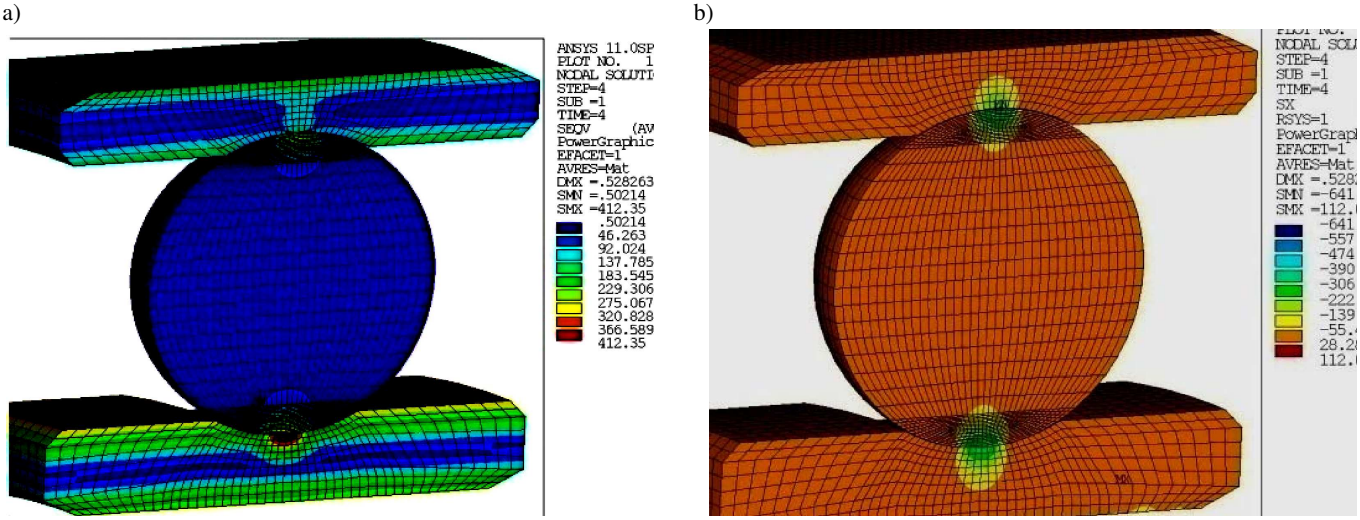

Fig. 11. Cross-section on the major axis of the generator: a) Huber-Mises stresses, b) radial stresses

a) b)

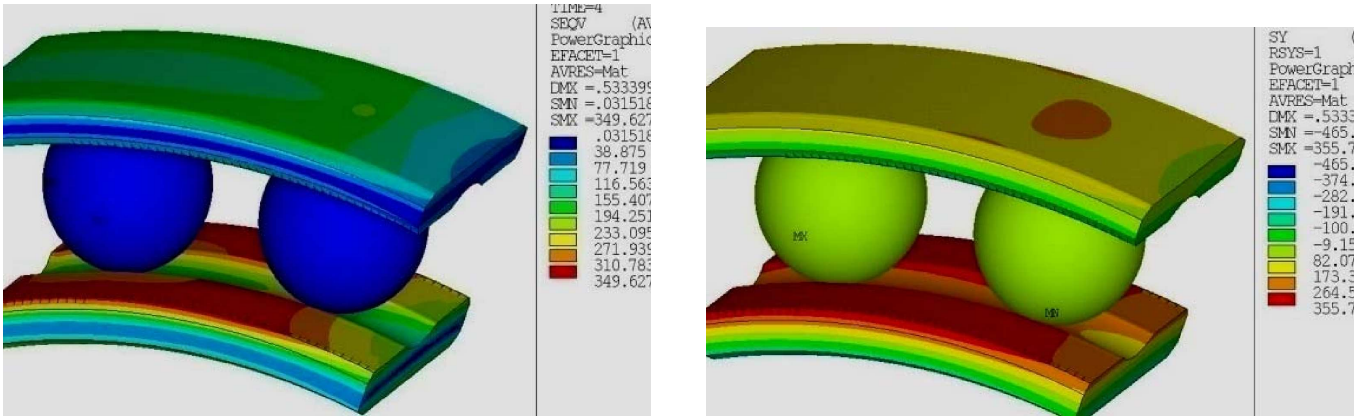

Fig. 12. Stresses: a) Huber-Mises, b) circumferential

a) b)

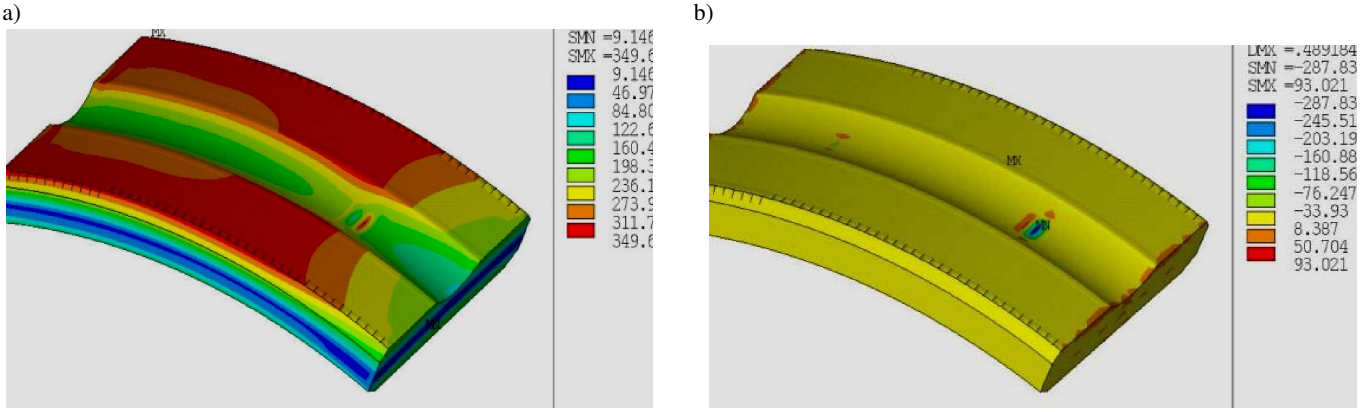

Fig. 13. Stresses on the inside running track: a) Huber-Mises, b) radial

a) b)

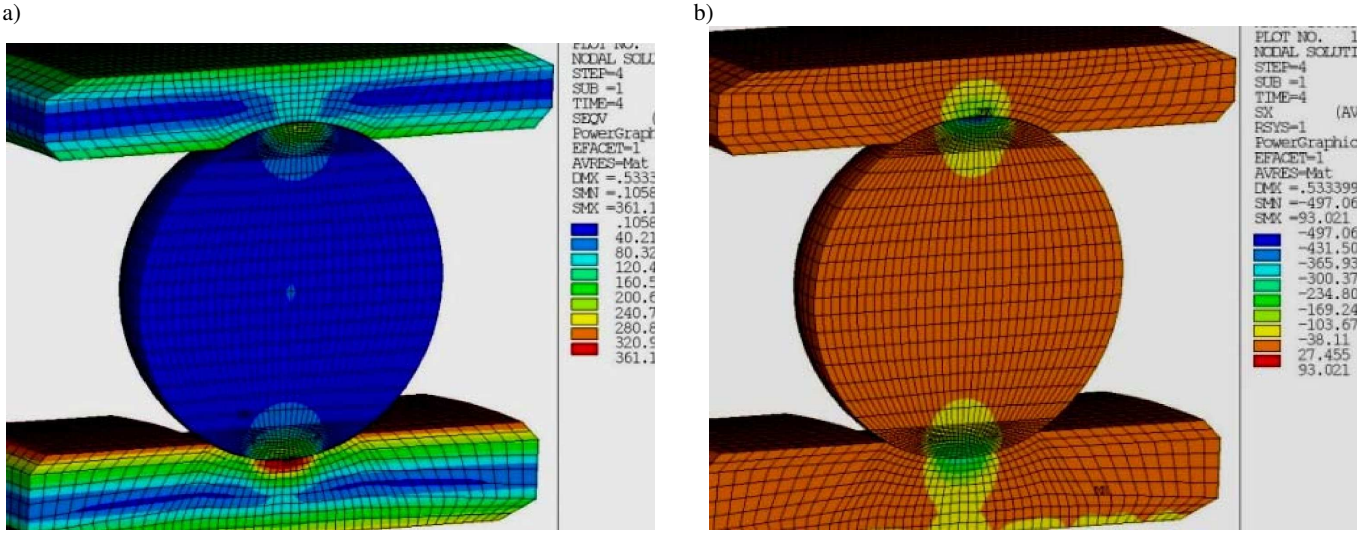

Fig. 14. Cross-section on the major axis of the generator: a) Huber-Mises stresses, b) radial stresses

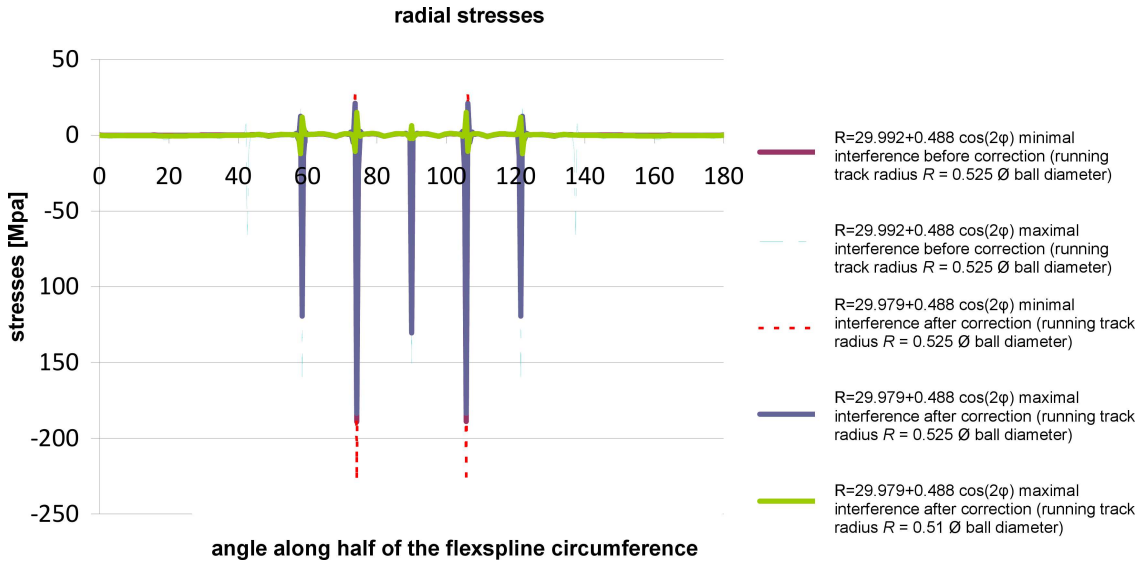

Fig. 15. Surface radial stresses on the internal ring of the flexible bearing

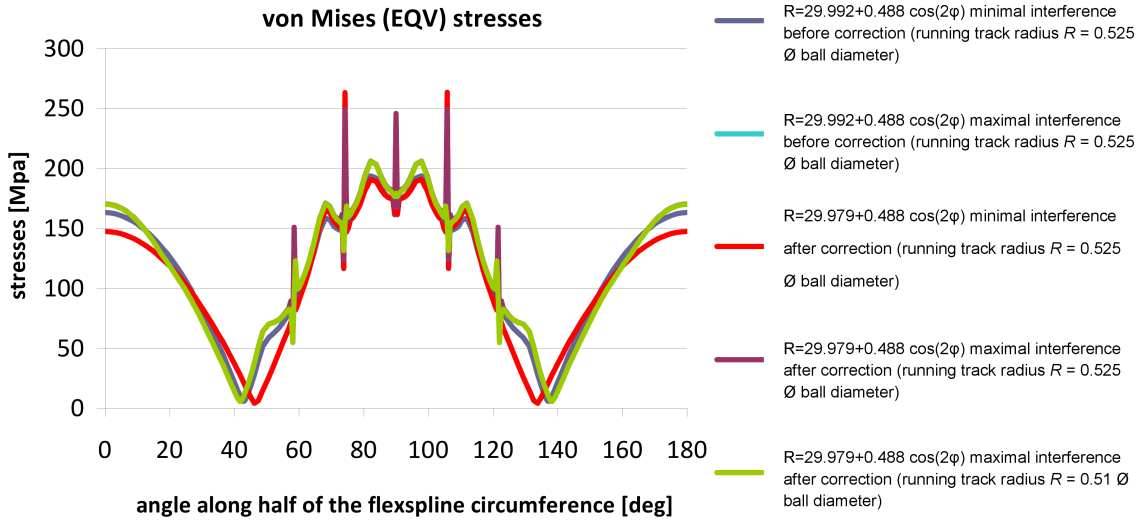

Fig. 16. Equivalent stresses in the running track of the external ring of the flexible bearing

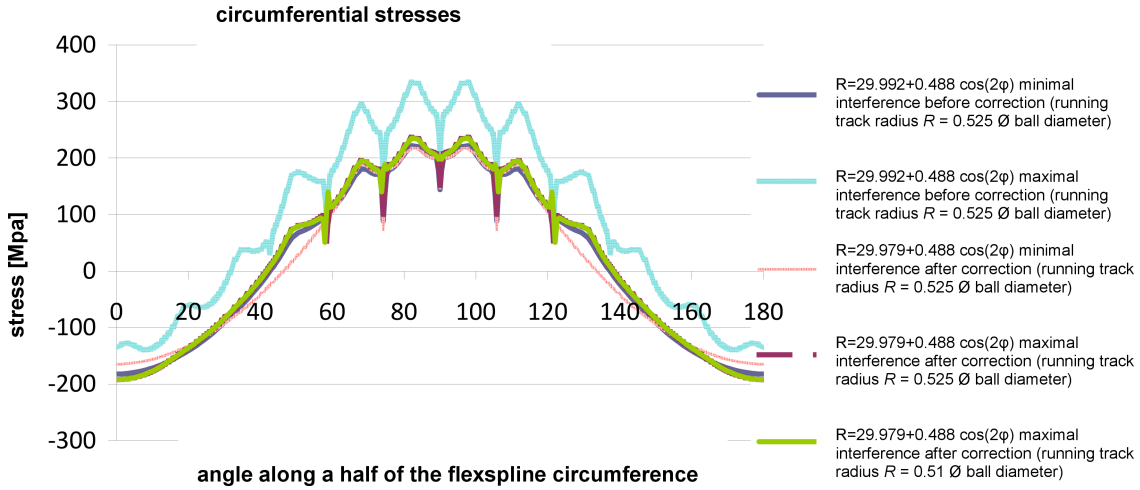

Fig. 17. Equivalent stresses in the running track of the internal ring of the flexible bearing

FEM simulation results ($R = 29.979 + 0.488\cos(2\phi)$ maximum interference after correction of the fit $R^{0.01}_{0.001}$, $R_{run} = 0.515 * \phi_{ball}$).

The analysis of the obtained simulation results for stresses in the generator bearing before and after correction of the bearing-cam association and correction of the running track radius (Figs. 8–17) indicates a considerable drop of the maximum stresses, both the directional and the equivalent. Because of the vastness of the numerical data, only the limiting states of the associations with the minimal interference before correction and the maximal one after it are presented. The introduced modifications produced noticeable drop of stresses of the least advantageous association after correction in comparison with the best one before it. The maximum equivalent Huber-Mises stresses shown in Figs. 11, 14 and 15–17 dropped by 51 MPa. The introduced modifications in tolerances of cams and running track radii eliminated subsequent cases of cracking of the bearing rings and resulting damage of harmonic drives. Technology of 8 series of dimensions of flexible rolling bearings has been prepared and implemented [3]. The production is now on, targeted at the UE countries.

4. Mathematical model of the flexspline of a harmonic drive

The essential element of proper performance of a harmonic drive is correct assembly of the generator cam with the flexspline. Having assumed the correct geometrical parameters of the flexspline and toothed ring, it is important to maintain properly chosen radial deformation and fit of the generator bearing in the flexspline. Excessive interference introduces normal stresses from the tensioned flexspline. On the other hand, excessive clearance lowers loading capability of the drive and diminishes the limiting torque at which teeth begin to skip. Also the length-to-diameter ration of the flexspline has considerable effect on the normal bending and tensile stresses being transferred to the flexspline bottom.

The investigations were carried out on a mathematical model describing the stress state in the flexspline in function of the radial deviation w^* as well as length and height of the flexpline bottom. 3D numerical simulations based on a FEM model were realized. The flexsline was modelled as a Kirchhoff-Love cylindrical shell, whereas the bottom as a annular plate. At the free edge of the shell, a displacement w^* is assumed due to interaction with the cam, while the plate axis is simply supported. The shell and plate are permanently joined (ideal mechanical contact). The equation of forces and moments balance for the cylindrical shell are:

$$\begin{gathered}
\frac{\partial N_{1t}}{\partial z} - \frac{1}{R}\frac{\partial S_{12}}{\partial \theta} = 0, \\
\frac{1}{R}\frac{\partial N_{2t}}{\partial \theta} + \frac{\partial S_{12}}{\partial z} + \frac{1}{R}\left(\frac{1}{R}\frac{\partial M_{2t}}{\partial \theta} + 2\frac{\partial H_{12}}{\partial z}\right) = 0, \\
N_{2t} - R\frac{\partial}{\partial z}\left(\frac{\partial M_{1t}}{\partial z} + \frac{1}{R}\frac{\partial H_{12}}{\partial \theta}\right) - \\
- \frac{\partial}{\partial \theta}\left(\frac{1}{R}\frac{\partial M_{2t}}{\partial \theta} + \frac{\partial H_{12}}{\partial z}\right) = \frac{\partial M_{2t}}{\partial \theta},
\end{gathered} \tag{6}$$

where R is the radius of the middle surface of the shell, z – coordinate along the shell axis measured from the free edge deformed by the cam $(0 \le z \le l)$; θ- circular coordinate. The forces and moments are expressed by components of deformation of the middle surface as:

$$\begin{gathered}
N_{1t} = \frac{D_{0t}}{1-\nu^2}\left(\varepsilon_1 + \nu\varepsilon_2\right), \\
N_{2t} = \frac{D_{0t}}{1-\nu^2}\left(\varepsilon_2 + \nu\varepsilon_1\right), \\
M_{1t} = D_{1t}\left(\kappa_1 + \nu\kappa_2\right), \\
M_{2t} = D_{1t}\left(\kappa_2 + \nu\kappa_1\right), \\
S_{12} = \frac{D_{0t}}{1+\nu}\varepsilon_{12}, \\
H_{12} = D_{1t}\left(1-\nu\right)\kappa_{12}.
\end{gathered} \tag{7}$$

The deformation components of the middle surface are in relation with its axial displacement u_1 and the transverse one w:

$$\begin{aligned}
\varepsilon_1 &= \frac{\partial u_1}{\partial z}, \\
\varepsilon_2 &= \frac{1}{R}\frac{\partial u_2}{\partial \theta} + \frac{w_t}{R}, \\
\varepsilon_{12} &= \frac{1}{2}\left(\frac{1}{R}\frac{\partial u_1}{\partial \theta} + \frac{\partial u_2}{\partial z}\right), \\
\kappa_1 &= -\frac{\partial^2 w_t}{\partial z^2}, \\
\kappa_2 &= -\frac{1}{R^2}\frac{\partial}{\partial \theta}\left(\frac{\partial w_t}{\partial \theta} - u_2\right), \\
\kappa_{12} &= -\frac{1}{R}\frac{\partial}{\partial z}\left(\frac{\partial w_t}{\partial \theta} - u_2\right).
\end{aligned} \tag{8}$$

At the same time, the integrity equations have the form:

$$\begin{aligned}
&\frac{\partial \kappa_2}{\partial z} - \frac{1}{R}\frac{\partial \kappa_{12}}{\partial \theta} = 0, \\
&\frac{\partial \kappa_1}{\partial \theta} - R\frac{\partial \kappa_{12}}{\partial z} - \frac{1}{R}\frac{\partial \varepsilon_1}{\partial \theta} + 2\frac{\partial \varepsilon_{12}}{\partial z} = 0, \\
&\kappa_1 + R\frac{\partial}{\partial z}\left(\frac{\partial \varepsilon_2}{\partial z} - \frac{1}{R}\frac{\partial \varepsilon_{12}}{\partial \theta}\right) + \\
&+ \frac{\partial}{\partial \theta}\left(\frac{1}{R}\frac{\partial \varepsilon_1}{\partial \theta} - \frac{\partial \varepsilon_{12}}{\partial z}\right) = 0.
\end{aligned} \tag{9}$$

In this case, the stresses in the cylindrical shell are as follows:

$$\begin{aligned}
\sigma_z &= \frac{1}{2h}\left(N_{1t} + 3\frac{\gamma}{h^2}M_{1t}\right), \\
\sigma_\theta &= \frac{1}{2h}\left(N_{2t} + 3\frac{\gamma}{h^2}M_{2t}\right), \\
\sigma_{z\theta} &= \frac{1}{2h}\left(S_{12} + 3\frac{\gamma}{h^2}H_{12}\right),
\end{aligned} \tag{10}$$

where $2h$ is the shell thickness, $-h \le \gamma \le h$. Substituting (7) and (8) into (6), one obtains the equilibrium equations in terms of displacements:

$$\begin{aligned}
&\frac{D_{0t}}{1-\nu^2}\left[\frac{\partial^2 u_1}{\partial z^2} + \frac{\nu}{R}\left(\frac{\partial^2 u_2}{\partial z \partial \theta} + \frac{\partial w_t}{\partial z}\right)\right] - \\
&- \frac{D_{0t}}{2R(1+\nu)}\left(\frac{\partial^2 u_1}{\partial \theta^2} + \frac{\partial^2 u_2}{\partial \theta \partial z}\right) = 0, \\
&\frac{1}{R}\frac{D_{0t}}{(1-\nu^2)}\left[\frac{1}{R}\left(\frac{\partial^2 u_2}{\partial \theta^2} + \frac{\partial w_t}{\partial \theta}\right) + \nu\frac{\partial^2 u_1}{\partial \theta \partial z}\right] + \\
&+ \frac{D_{0t}}{2(1+\nu)}\left(\frac{1}{R}\frac{\partial^2 u_1}{\partial z \partial \theta} + \frac{\partial^2 u_2}{\partial z^2}\right) - \\
&- \frac{D_{1t}}{R^2}\left[\frac{1}{R^2}\frac{\partial^2}{\partial \theta^2}\left(\frac{\partial w_t}{\partial \theta} - u_2\right) + \nu\frac{\partial^3 w_t}{\partial \theta \partial z^2}\right] - \\
&- \frac{2D_{1t}(1-\nu)}{R^2}\frac{\partial^2}{\partial z^2}\left(\frac{\partial w_t}{\partial \theta} - u_2\right) = 0, \\
&\frac{D_{0t}}{1-\nu^2}\left(\frac{1}{R}\frac{\partial u_2}{\partial \theta} + \frac{w_t}{R} + \nu\frac{\partial u_1}{\partial z}\right) + \\
&+ D_{1t}R\left[\frac{\partial^4 w_t}{\partial z^4} + \frac{\nu}{R^2}\left(\frac{\partial^4 w_t}{\partial z^2 \partial \theta^2} - \frac{\partial^3 u_2}{\partial z^2 \partial \theta}\right)\right] + \\
&+ \frac{2D_{1t}(1-\nu)}{R}\frac{\partial^3}{\partial \theta \partial z^2}\left(\frac{\partial w_t}{\partial \theta} - u_2\right) + \\
&+ \frac{D_{1t}}{R}\left[\frac{1}{R^2}\frac{\partial^3}{\partial \theta^3}\left(\frac{\partial w_t}{\partial \theta} - u_2\right) + \nu\frac{\partial^4 w_t}{\partial z^2 \partial \theta^2}\right] = \\
&= -D_{1t}\left[\frac{1}{R^2}\frac{\partial^2}{\partial \theta^2}\left(\frac{\partial w_t}{\partial \theta} - u_2\right) + \nu\frac{\partial^3 w_t}{\partial \theta \partial z^2}\right],
\end{aligned} \tag{11}$$

where $D_{0t} = 2Eh$ is the tensile stiffness, $D_{1t} = \frac{2}{3}\frac{Eh^3}{(1-\nu^2)}$ – bending stiffness, ν – Poisson's ratio. The boundary conditions for the shell are:

$$\begin{aligned}
&\text{at the edge } z = 0 : w_t = w_*, \;\; M_{1t} = 0, \;\; N_{1t} = 0. \\
&\text{at the edge } z = l \text{ – ideal mechanical contact} \\
&\qquad\qquad \text{with the annular plate.}
\end{aligned} \tag{12}$$

In the axi-symmetric case (u_2 and derivatives with respect to θ are zero), system of equations (11) assumes the form:

$$\begin{aligned}
&\frac{\partial^2 u_1}{\partial z^2} + \frac{\partial w_t}{\partial z} = 0, \\
&\frac{D_{0t}}{1-\nu^2}\left(\frac{w_t}{R} + \nu\frac{\partial u_1}{\partial z}\right) + D_{1t}R\frac{\partial^4 w_t}{\partial z^4} = 0
\end{aligned} \tag{13}$$

and the second equation in (11) is satisfied by identity. Having integrated the first equation in (11) and substituted it in the place of the second one, we arrive at:

$$\frac{d^4 w_t}{dz^4} + \frac{3\left(1-\nu^2\right)}{h^2 R^2}w_t = 0. \tag{14}$$

After introducing non-dimensional quantities:

$$w_0 = \frac{w_t}{R}, \qquad x = \frac{az}{R}, \qquad a^4 = \frac{3\left(1-\nu^2\right)R^2}{4h^2} \tag{15}$$

equation (14) assumes the form:

$$\frac{d^4 w_0}{dx^4} + 4w_0 = 0. \tag{16}$$

The general solution to this equation is sought in the exponential form $w_0 = e^{tx}$. Then, for the characteristic equation $t^4+4=0$ the following roots are found: $t_1 = 1+i$, $t_2 = 1-i$, $t_3 = -1+i$, $t_4 = -1-i$. Solution to equation (11) can be expressed as:

$$w_0 = Ae^x \cos x + Be^x \sin x + Ce^{-x}\cos x + De^{-x}\sin x, \tag{17}$$

where the coefficients A, B, C, D are found from the boundary conditions. In the general case, formulas for the forces and moments (7), taking into account (15), are following:

$$\begin{aligned} N_{1t} &= 0, \qquad S_{12} = 0, \\ H_{12} &= 0, \qquad N_2 = D_{0t} w_0, \\ M_{1t} &= -\frac{D_{0t}R}{4a^2}\frac{d^2 w_0}{dx^2}, \qquad M_{2t} = \nu M_{1t}. \end{aligned} \tag{18}$$

Stresses (10) in the shell can be now described as:

$$\begin{aligned} \sigma_z^{=} &- \frac{3D_{0t}R\gamma}{8a^2h^3}\frac{d^2 w_0}{dx^2}, \\ \sigma_\theta^{=} &\frac{1}{2h}\left(N_{2t} + 3M_{2t}\frac{\gamma}{h^2}\right). \end{aligned} \tag{19}$$

The maximum stress on the outer "+" and inner "-" surface are obtained for $\gamma = \pm h$, hence

$$\sigma_z^{\pm} = \mp\frac{3D_{0t}R}{8a^2h^2}\frac{d^2 w_0}{dx^2}, \qquad \sigma_\theta^{\pm} = \frac{D_{0t}}{2h}w_0 + \nu\sigma_z^{\pm}.$$

According to formulas (17) and (18), we obtain:

$$\begin{aligned} M_{1t} &= -\frac{D_{0t}R}{2a^2}\left[e^x\left(B\cos x - A\sin x\right)\right. \\ &\left. + e^{-x}\left(C\sin x - D\cos x\right)\right], \\ Q &= -\frac{D_{0t}}{2a}\left[Be^x\left(\cos x - \sin x\right) - Ae^x\left(\sin x + \cos x\right)\right. \\ &\left. - Ce^{-x}\left(\sin x - \cos x\right) + De^{-x}\left(\sin x + \cos x\right)\right], \\ \frac{dw_0}{dx} &= \left[Ae^x\left(\cos x - \sin x\right) + Be^x\left(\sin x + \cos x\right)\right. \\ &\left. - Ce^{-x}\left(\sin x + \cos x\right) - De^{-x}\left(\sin x - \cos x\right)\right], \\ \frac{d^2 w_t}{dx^2} &= 2\left[e^x\left(B\cos x - A\sin x\right)\right. \\ &\left. + e^{-x}\left(C\sin x - D\cos x\right)\right], \end{aligned} \tag{20}$$

where Q is the shear force. Formulas (20) will be used for the boundary conditions. In particular, fulfilling conditions (12), we find that: $B = D$, $C = \frac{w_*}{R} - A$. Then, formulas (20) can be expressed as:

$$\begin{aligned} M_{1t} &= -\frac{D_{0t}R}{a^2}\left(Bshx\cos x - Achx\sin x + \frac{w_*}{2R}e^{-x}\sin x\right), \\ Q &= -\frac{D_{0t}}{a}\Big[B\left(chx\cos x - shx\sin x\right) \\ &- A\left(chx\cos x + shx\sin x\right) + \frac{w_*}{2R}e^{-x}\left(\cos x - \sin x\right)\Big], \\ \frac{dw_0}{dx} &= 2A\left(\cos x chx - \sin x shx\right) + \\ &+ 2B\left(\cos x chx + \sin x shx\right) - \frac{w_*}{R}e^{-x}\left(\cos x + \sin x\right), \\ \frac{d^2 w_t}{dx^2} &= 4Bshx\cos x - 4Achx\sin x + 2\frac{w_*}{R}e^{-x}\sin x \end{aligned} \tag{20'}$$

and the bending: $w_0 = 2Ashx\cos x + 2Bchx\sin x + \frac{w_*}{R}e^{-x}\cos x$. The equilibrium equations for the annular plate modelling the flexspline bottom are:

$$\begin{aligned} \frac{d^2 u}{dr^2} + \frac{1}{r}\frac{du}{dr} - \frac{u}{r^2} &= 0, \\ \frac{d^3 w_p}{dr^3} + \frac{1}{r}\frac{d^2 w_p}{dr^2} - \frac{1}{r^2}\frac{dw_p}{dr} &= 0. \end{aligned} \tag{21}$$

The forces and moments expressed in terms of the displacements u and w_p are described as:

$$\begin{aligned} N_{1p} &= \frac{D_{0p}}{1-\nu^2}\left(\frac{du}{dr} + \nu\frac{u}{r}\right), \\ N_{2p} &= \frac{D_{0p}}{1-\nu^2}\left(\frac{u}{r} + \nu\frac{du}{dr}\right), \\ M_{1p} &= -D_{1p}\left(\frac{d^2 w_p}{dr^2} + \frac{\nu}{r}\frac{dw_p}{dr}\right), \\ M_{2p} &= -D_{1p}\left(\frac{1}{r}\frac{dw_p}{dr} + \nu\frac{d^2 w_p}{dr^2}\right). \end{aligned} \tag{22}$$

The radial and circumferential stresses in the plate:

$$\begin{aligned} \sigma_r &= \frac{1}{2h_1}\left(N_{1p} + 3\frac{\gamma}{h_1^2}M_{1p}\right), \\ \sigma_\varphi &= \frac{1}{2h_1}\left(N_{2p} + 3\frac{\gamma}{h_1^2}M_{2p}\right), \end{aligned} \tag{23}$$

where $D_{0p} = 2Eh_1$ is the tensile stiffness, $D_{1p} = \frac{2}{3}\frac{Eh_1^3}{(1-\nu^2)}$ – bending stiffness, h_1 – plate thickness ($-h_1 \le \gamma \le +h_1$), ($b \le r \le d$), $d = R - 2h$. The solution to equation (21) can be expressed in the form:

$$u = C_1 r + \frac{C_2}{r}, \qquad w_p = C_3 \ln r + C_4 + C_5 r^2. \tag{24}$$

Boundary conditions for the plate:

$$\left.\begin{array}{l} u=0, \\ M_{1p}=0 \end{array}\right\} \quad \text{at} \quad r=b, \tag{25}$$

at $r=d$ – ideal mechanical contact with the shell.

$$\begin{gathered} u(d)=w_t(l), \\ \frac{dw_p(d)}{dr}=\frac{dw_t(l)}{dz}, \\ N_{1p}(d)=Q(l), \\ M_{1p}(d)=M_{1t}(l). \end{gathered} \tag{26}$$

Satisfying conditions (12), (25), (26), we obtain the following system of equations:

$$\begin{gathered} C_3\frac{1}{a}\left[\frac{1}{d}+\frac{(1-\nu)d}{(1+\nu)b^2}\right]- \\ -2\left[A(\cos\beta ch\beta-\sin\beta sh\beta)+\right. \\ \left.+B(\cos\beta ch\beta+\sin\beta sh\beta)\right]= \\ =-\frac{w_*}{R}e^{-\beta}(\cos\beta+\sin\beta), \\ C_1\left(\frac{d^2-b^2}{Rd}\right)-2A\cos\beta sh\beta-2B\sin\beta ch\beta+ \\ =\frac{w_*}{R}e^{-\beta}\cos\beta, \\ C_1\frac{2ah_1}{(1-\nu^2)h}\left[1+\nu-\frac{b^2(\nu-1)}{d^2}\right]+ \\ +2A(\sin\beta sh\beta+\cos\beta sh\beta)+ \\ +2B(\sin\beta sh\beta-\cos\beta ch\beta)= \\ =\frac{w_*}{R}e^{-\beta}(\cos\beta-\sin\beta), \\ C_3\frac{2a^2h_1^3}{3(1-\nu^2)hR}\left(\frac{\nu-1}{d^2}+\frac{1-\nu}{b^2}\right)+ \\ +2A\sin\beta ch\beta-2B\cos\beta sh\beta=\frac{w_*}{R}e^{-\beta}\sin\beta \\ \left(\beta=\frac{al}{R}\right). \end{gathered} \tag{27}$$

From boundary condition (25) it ensues that

$$C_2=-C_1b^2, \qquad C_5=\frac{1-\nu}{2(1+\nu)b^2}C_3$$

and from condition (12) that

$$B=D, \qquad C=A-\frac{w_*}{R}.$$

Thus, solving the system of equations (27), we obtain:

$$\begin{gathered} A=\frac{1}{L}\left[(n\psi-ps)(k\delta-t\xi)+(\alpha\xi+\lambda\delta)(pq-mn)\right], \\ B=\frac{1}{L}\left[(n\psi-ps)(q\xi+m\delta)+(nk+pt)(\alpha\xi+\lambda\delta)\right], \\ L=(pq-mn)(q\xi+m\delta)-(nk+pt)(k\delta-t\xi), \\ C_1=\frac{1}{n}(s-At+Bq), \\ C_3=\frac{1}{\delta}(Aq+Bt-\alpha), \end{gathered} \tag{28}$$

where

$$\begin{gathered} k=2sh\beta\cos\beta, \qquad m=2ch\beta\sin\beta, \\ q=2(ch\beta\cos\beta-sh\beta\sin\beta), \\ t=2(ch\beta\cos\beta+sh\beta\sin\beta), \\ s=\frac{w_*}{R}e^{-\beta}(\cos\beta-\sin\beta), \\ \alpha=\frac{w_*}{R}e^{-\beta}(\cos\beta+\sin\beta), \\ \psi=\frac{w_*}{R}e^{-\beta}\cos\beta, \\ \lambda=\frac{w_*}{R}e^{-\beta}\sin\beta, \\ \xi=\frac{2a^2h_1^3}{3(1-\nu^2)hR}\left(\frac{\nu-1}{d^2}+\frac{1-\nu}{b^2}\right), \\ p=\frac{1}{R}\left(d-\frac{b^2}{d}\right), \\ n=\frac{2ah_1}{(1-\nu^2)h}\left[1+\nu-\frac{b^2(\nu-1)}{d^2}\right], \\ x=\frac{az}{R}, \\ a=\sqrt[4]{\frac{3(1-\nu^2)R^2}{4h^2}}, \\ \delta=\frac{1}{a}\left[\frac{1}{d}+\frac{(1-\nu)}{(1+\nu)}\frac{d}{b^2}\right], \\ \beta=\frac{al}{R}, \qquad (0\le z\le l). \end{gathered}$$

The maximum stress on the outer "+" and inner "−" surface of the shell are obtained basing on Eqs. (19′), (20′):

$$\begin{gathered} \sigma_z^{\pm}=\pm\frac{3ER}{a^2h}\left(Achx\sin x-Bshx\cos x-\frac{w_*}{2R}e^{-x}\sin x\right), \\ \sigma_\theta^{\pm}= \\ =E\left[2Ashx\cos x+2Bchx\sin x+\frac{w_*}{R}e^{-x}\cos x\right]+\nu\sigma_z^{\pm}. \end{gathered} \tag{29}$$

The maximum stress on the outer "+" and inner "−" surface of the shell are obtained basing on Eq. (23) at $\gamma = \pm h$:

$$\sigma_r^{\pm} = \frac{E}{(1-\nu^2)}\left\{C_1\left[1+\nu+\frac{b^2}{r^2}(1-\nu)\right]\right.$$
$$\left.\mp C_3\left(\frac{\nu-1}{r^2}+\frac{1-\nu}{b^2}\right)\right\},$$
$$\sigma_\varphi^{\pm} = \frac{E}{(1-\nu^2)}\left\{C_1\left[1+\nu+\frac{b^2}{r^2}(\nu-1)\right]\right. \tag{30}$$
$$\left.\mp C_3\left(\frac{1-\nu}{r^2}+\frac{1-\nu}{b^2}\right)\right\}.$$

Results of numerical calculations for the stresses in the flexspline versus its length, height, bottom thickness and the interference in the flexspline-generator bearing fit are shown in Figs. 18–20. As can be seen, the positive deviation $w*$ (interference) in the flexspline-generator bearing fit increases normal stresses coming from tensile loading of the flexspline. The shell was simulated for a deformation increment from the deviation (interference) in the fit. Resultant stresses induced by the generator deformation and the interference were found for the 3D FEM model. For ultra-short flexsplines, the stresses in the bottom part rapidly grow. Practically, the bottom carries all normal forces coming form tension, which is illustrated in Fig. 19b. The bottom thickness for the assumed deformation forces in the simulation range 2–5 mm does not essentially affect the magnitude of radial stresses in this element (see Fig. 20).

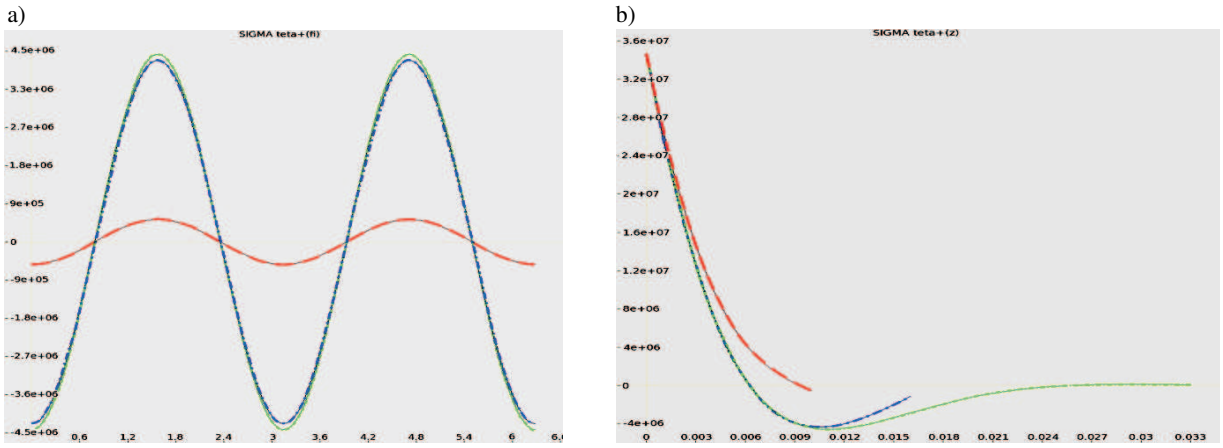

Fig. 18. Circumferential stresses on the outer surface of the flexspline for $w* = 0.002\cos 2\varphi$, a) vs. φ for $z = 0.005$ m, b) along z axis for $\varphi = 0$

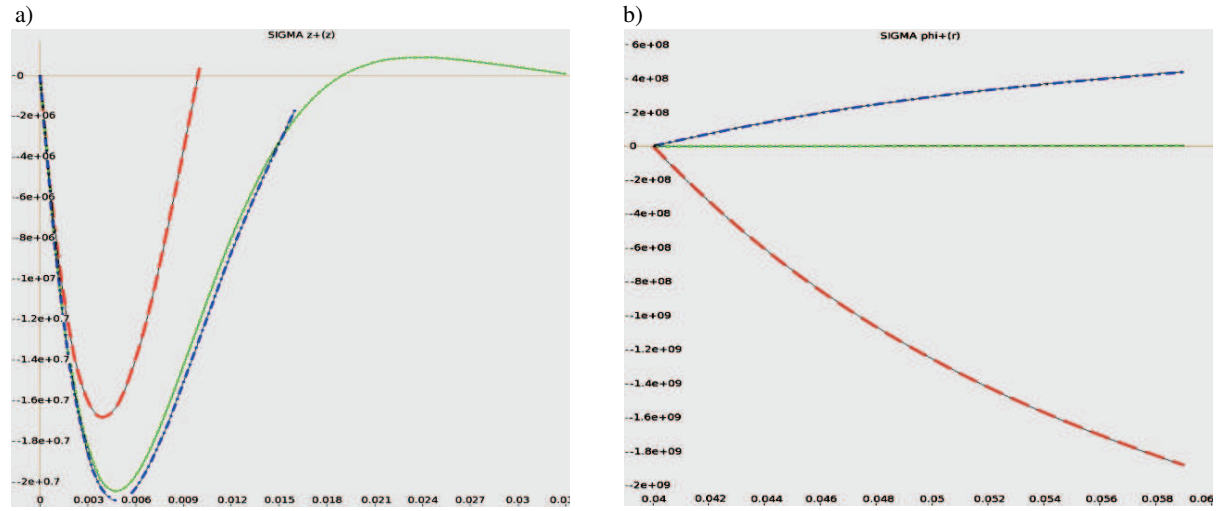

Fig. 19. a) Axial stresses in the flexspline for $\varphi = 0$, b)Circumferential stresses in the bottom vs. r for $w* = 0.2 + 0.002\cos 2\varphi$

a) b)

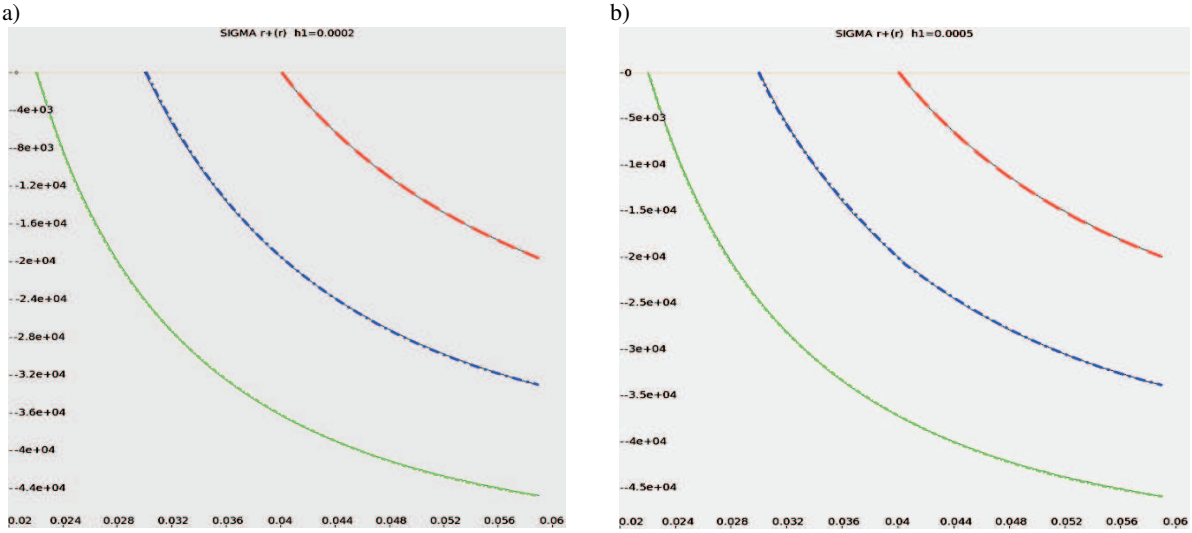

Fig. 20. Radial stresses in the bottom vs. r for the bottom thickness a) $h_1 = 0.2$ mm, b) $h_1 = 0.5$ mm, where the colours are for the following length-to-diameter ratios of the flexspline $L/D = 0.1$ (red), $L/D = 0.15$ (blue), $L/D = 0.275$ (green)

5. FEM analysis of the 3D flexspline model

The numerical simulations were carried out for the following values of the radial interference: $w* = 0$ mm, 0.01 mm, 0.02 mm and standard lengths of the harmonic drive $L = 0.7D$, $L = 0.3D$, $L < 0.3D$, where D denotes the diameter of the flexspline (Figs. 21–23). Simulations were realised for the deformation $w - m = 0.5$ mm.

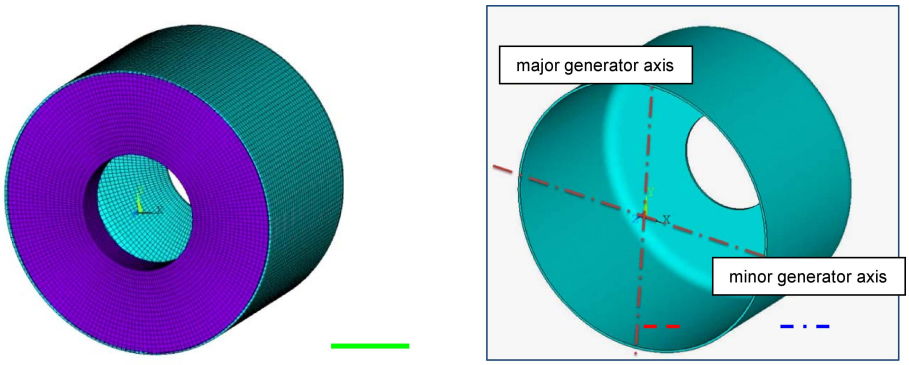

Fig. 21. 3D model of the flexspline corresponding to the mathematical description

a) b)

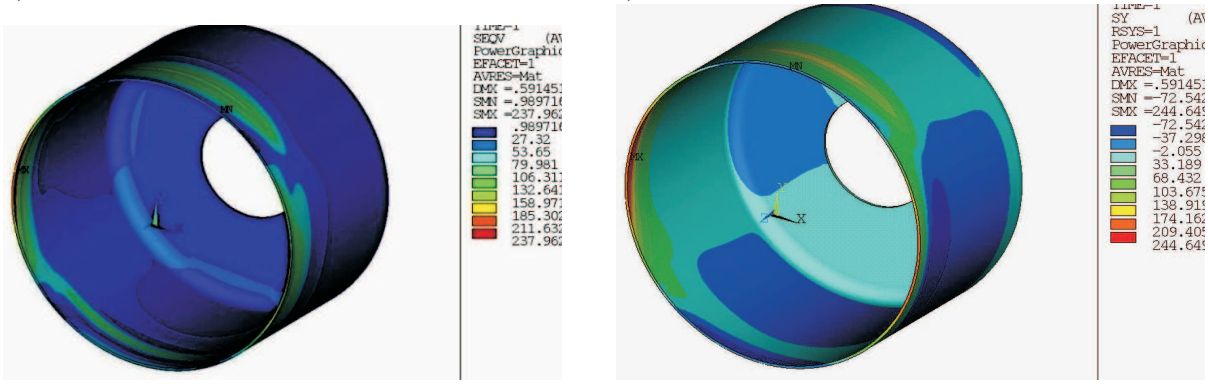

Fig. 22. Stresses: a) Huber-Mises, b) circumferential for $D = 120$ mm, $L = 75$ mm, $g = 1$ mm, $m = 0.5$ mm, $R(\varphi) = d/2 + m * \cos 2\varphi$, $w* = 0$

a) b)

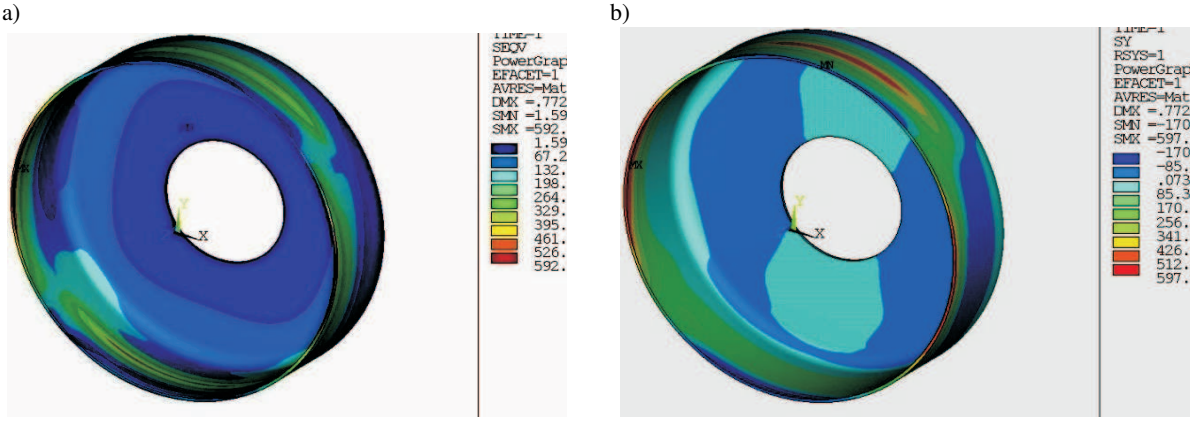

Fig. 23. Stresses: a) Huber-Mises, b) circumferential for $D = 120$ mm, $L = 33$ mm, $g = 1$ mm, $m = 0.5$ mm, $R(\varphi) = (d/2 + w*) + m * \cos 2\varphi$, $w* = 0.02$ mm

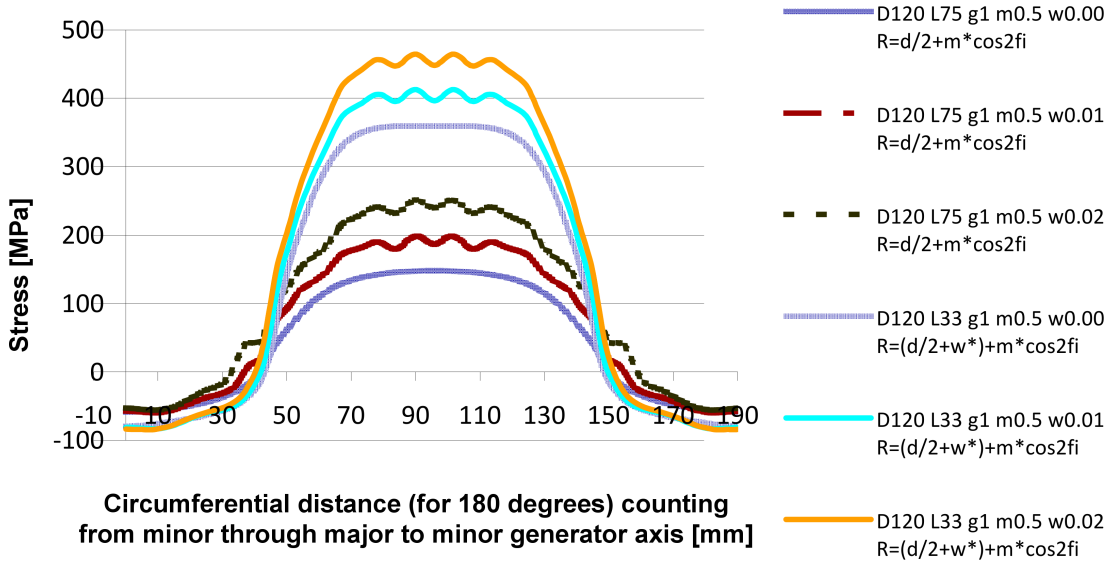

Fig. 24. Huber-Mises stresses on a half of the flexspline circumference

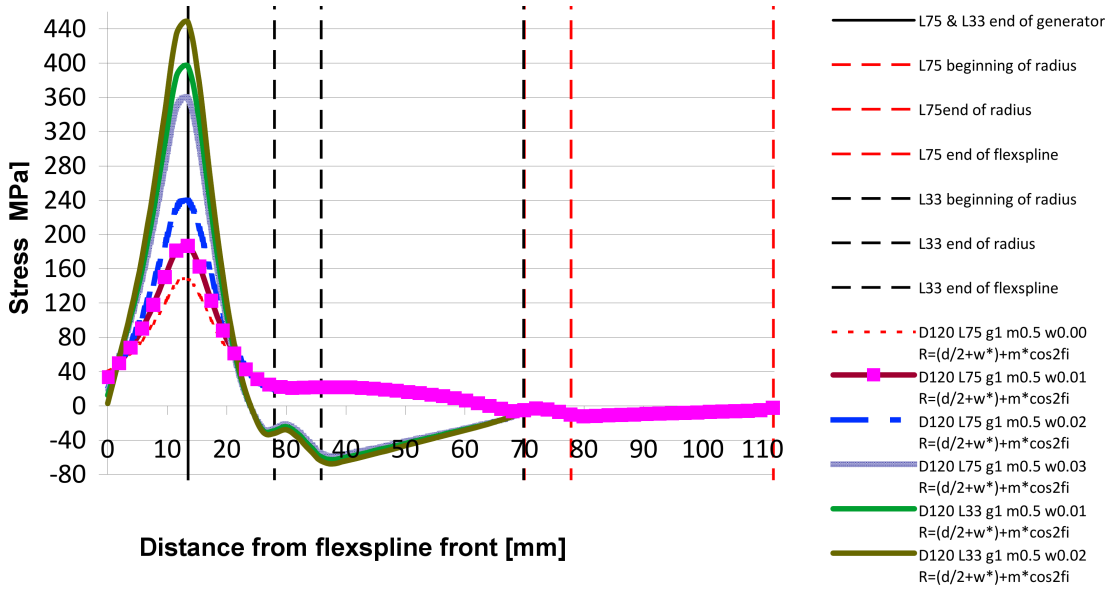

Fig. 25. Circumferential stresses along the flexspline axis

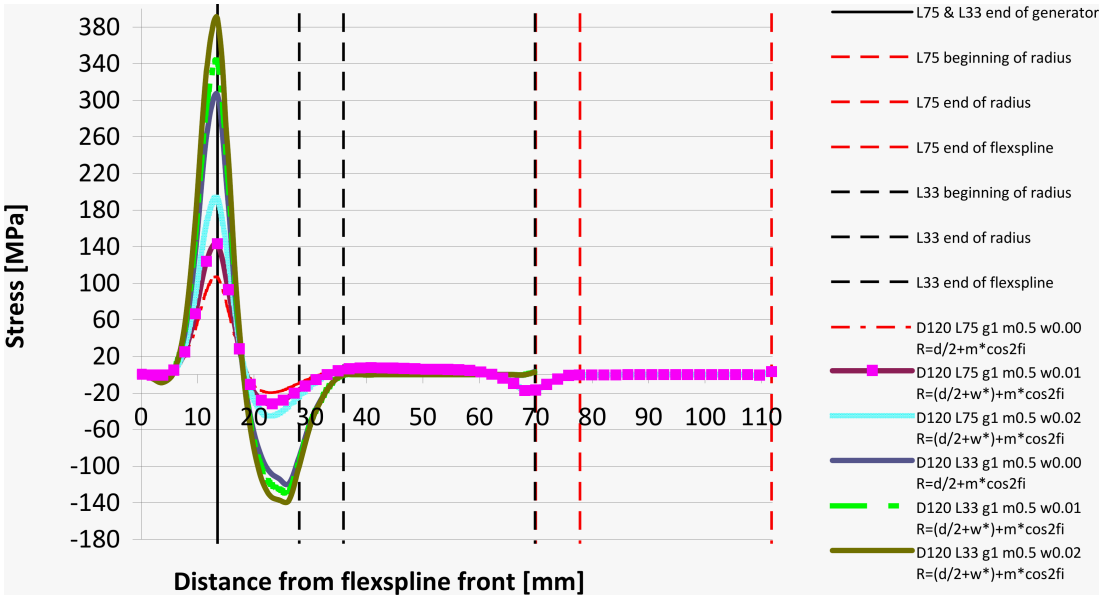

Fig. 26. Axial stresses along the flexspline length

Analysis of the obtained from simulations stresses versus length and radial deformation of the flexspline as well as deviation of the fit in the generator indicate a linear relationship of the stress increment both directional and equivalent with respect to the shortening of the flexspline length. Also introduction of the positive radial deviation of 0.01 mm increased the magnitude of equivalent stresses by about 20% (Fig. 24) for $L/D = 0.75$. On the other hand, for a short flexspline of $L/D = 0.33$, the stress increment for the same deviation of fit remained unchanged in magnitude but relatively dropped with respect to resultant stresses in the shortened flexslpine (see Figs. 24–26).

6. Summary

The analysis of the generator-flexspline system carried out on a mathematical model as well as through FEM simulations and test-stand experiments pointed out considerable effect of the generator bearing fit in the cam and flexspline on the stress state in the bearing and the flexpline. The cam should be manufactured and fitted to the bearing with a clearance of 0–0.015 mm on the diameter. This enables maintaining sufficient radial gap for the generator bearing under loading and preserves sufficient elasto-frictional association with respect to instantaneous two-fold overloading of the harmonic drive. The maximum radial and equivalent stresses appear in running tracks of both rings at the contact with the nearest rolling elements symmetrically placed on both sides of the major cam axis, however not on the axis itself. The optimal radius of the running track in terms of the bearing stress state turned out to be R =0.51–0.515ϕk, not 0.525ϕk. The shortening of the flexspline length without structural changes in its design proportionally increases normal stresses both in the flexspline and its bottom. Extreme shortening of L/D =0.10–0.15 and maintaining the radial deformation in the bottom leads to the appearance of tensile stresses with damaging magnitude cracking the structure immediately or after a low number of loading cycles. For $L/D > 0.3$, it is possible to apply a fine-module meshing which would increase the ratio of the harmonic drive or introduce constructional modifications to the flexspline, e.g. outward flanging of the flexspline bottom or incorporate an optimised shape [1].

REFERENCES

[1] W. Ostapski and I. Mukha, "Stress state analysis of harmonic drive elements by FEM", *Bull. Pol. Ac.: Tech.* 55 (1), 115–123 (2007).

[2] W. Ostapski and A. Pisarek, "Simulation and test-stand examinations of load distribution in the mesh zone and generator contact of a single-stage harmonic drive", *Math. Franc.-Pol. Sem. Sci. Mech.* XVI, 84–102 (2008), (in Polish).

[3] W. Ostapski, "Implementation of technology of covering the elements of ordinary and elastic roller bearings with anti-wear coatings", *Report on National Target Project* 10T08012 2000C/5215, (2000), (in Polish).